Gravitational wave luminosity and net momentum flux in head-on mergers of black holes: Radiative patterns and mode mixing

Rafael Fernandes Aranha,[1,*] Ivano Damião Soares,[2,†] and Eduardo Valentino Tonini[3,‡]

[1]*Universidade do Estado do Rio de Janeiro—UERJ, 20550-900 Rio de Janeiro, Brazil*
[2]*Centro Brasileiro de Pesquisas Físicas—CBPF/MCTI, 22290-180 Rio de Janeiro, Brazil*
[3]*Instituto Federal do Espírito Santo—IFES, 29040-333 Vitória, Brazil*

(Received 19 January 2016; revised manuscript received 10 August 2016; published 8 September 2016)

We show that gravitational wave radiative patterns from a point test particle falling radially into a Schwarzschild black hole, as derived by Davis, Ruffini, Press and Price [M. Davis *et al.*, Phys. Rev. Lett. **27**, 1466 (1971).], are present in the nonlinear regime of head-on mergers of black holes. We use the Bondi-Sachs characteristic formulation and express the gravitational wave luminosity and the net momentum flux in terms of the news functions. We then evaluate the (-2)-spin-weighted ℓ-multipole decomposition of these quantities via exact expressions valid in the nonlinear regime and defined at future null infinity. Our treatment is made in the realm of Robinson-Trautman dynamics, with characteristic initial data corresponding to the head-on merger of two black holes. We consider mass ratios in the range $0.01 \leq \alpha \leq 1$. We obtain the exponential decay with ℓ of the total energy contributed by each multipole ℓ, with an accurate linear correlation in the log-linear plot of the points up to $\alpha \simeq 0.7$. Above this mass ratio the contribution of the odd modes to the energy decreases faster than that of the even modes, leading to the breaking of the linear correlation; for $\alpha = 1$ the energy in all odd modes is zero. The dominant contribution to the total radiated energy comes from the quadrupole mode $\ell = 2$ corresponding, for instance, to about $\simeq 84\%$ for small mass ratios up to $\simeq 99.8\%$ for the limit case $\alpha = 1$. The total rescaled radiated energy $E_W^{\text{total}}/m_0\alpha^2$ decreases linearly with decreasing α, yielding for the point particle limit $\alpha \to 0$ the value $\simeq 0.0484$, about 5 times larger than the result of Davis *et al.* [1]. The mode decomposition of the net momentum flux and of the associated gravitational wave impulses results in an adjacent-even-odd mode-mixing pattern. We obtain that the impulses contributed by each $(\ell, \ell+1)$ mixed mode also accurately satisfy the exponential decay with ℓ, for the whole mass ratio domain considered, $0.01 \leq \alpha < 1$. The (2, 3) mode contributions to the total impulses are dominant. The mode-mixing effect can also be seen in the decomposition of the net kick velocity imparted to the system by the gravitational wave emission. The mixed mode impulses reach a maximum at $\alpha \simeq 0.7$; for $\alpha > 0.7$ the impulses decrease and are zero in the equal mass case, due to the decrease to zero of the odd modes of the news functions.

DOI: 10.1103/PhysRevD.94.064017

I. INTRODUCTION

The collision and merger of two black holes are among the most promising astrophysical candidates for strong gravitational wave sources and are therefore of crucial interest for the present general efforts for direct observations of gravitational waves [2–5]. An accurate description of the radiative transfer processes involved in the emission of gravitational waves must take into account the full nonlinearity of the Einstein field equations. In the nonlinear regime, gravitational waves extract mass-energy, momentum and angular momentum of the source, and the radiative energy transfer involved in these processes may turn out to be fundamental for the astrophysics of black holes, such as the evolution and population of massive black holes in galaxies or in the intergalactic medium [6–8].

In the realm of general relativity the production and extraction of gravitational waves in processes involving black holes have been investigated basically within three complementary approaches, most of them connected to binary black hole inspirals: post-Newtonian (PN) approximations (cf. [9] and references therein), numerical relativity (NR) [10–14] and the close-limit approximation (CLA) supplemented with PN calculations [15,16], as well as combinations of these approaches. For the case of small mass ratios NR evaluations bridged with perturbation techniques were implemented in Refs. [13,17]. A particular class of black hole binaries, which are of particular interest for comparing and relating results from the various methods, are those with a very small mass ratio that can furnish tests for accuracy and for eventual validation of calculations made in extreme limits of the methods, as done for instance with the use of the effective-one-body approximation model (cf. [18–22]).

This is the case of a classical calculation in general relativity—the gravitational radiation from a point particle

*rafael.aranha@uerj.br
†ivano@cbpf.br
‡tonini@cefetes.br

falling radially into a Schwarzschild black hole [1]—some features of which extend naturally to the nonlinear regime of head-on mergers of nonspinning black holes with mass ratios $\alpha \geq 0.01$, as examined in this paper. The head-on case is a model problem that has the point particle case of [1] as a limit configuration when α approaches zero. We also examine the mode decomposition of the net momentum flux and the associated impulse of the gravitational waves emitted in the nonlinear regime for the same mass ratio range. These calculations were first made by Moncrief [23], considering the case of odd-parity quadrupole and octupole perturbations in collapsing relativistic stars. However, as in the present case of the axisymmetric head-on merger, odd-parity perturbations vanish as noted by Lousto and Price [24] in treating the first-order perturbation of the background of a Schwarzschild black hole by the radial infall of a particle.

Our treatment is based on the Bondi-Sachs (BS) energy-momentum conservation laws in the characteristic formulation [25–27], which regulate the gravitational wave radiative transfer processes of the system, in the realm of Robinson-Trautman (RT) spacetimes [28,29]. The characteristic initial data constructed for the RT dynamics already present a global apparent horizon, so the dynamics covers the post-merger phase of the system, which represents one of the most dynamic parts of the evolution, up to the final configuration of the remnant black hole [30].

We should mention that this formalism is distinct but complementary to the approaches using $1+3$ NR and PN approximations. Here we use physical quantities (the news functions and the BS four-momentum) defined only on characteristic surfaces $u = \text{const}$ and evaluated at future null infinity. Specifically, the physical importance of the BS four-momentum comes from the fact that, when an isolated system emits gravitational waves, its rate of change is directly related to the outward flux of the radiated energy and momentum by the gravitational waves. In this sense, here we have not treated a direct relation with the wave solutions used in $1+3$ NR and PN approaches, whose quantities are obtained from wave signals in time t evaluated at several spacelike spheres of extraction, and whose extension to future null infinity must be further implemented [31].

Of course, the physical results obtained in the characteristic formulation (using proper initial data) must give results consistent with other formulations. For instance, the initial data [Eq. (20)] result in an impressive agreement with the Fitchett distribution of the kick velocities as a function of the symmetric mass ratio [32,33], when compared to results obtained via post-Newtonian and $3+1$ NR techniques. Also, in [33] the initial data [Eq. (20)] was used (in the characteristic formulation) to show that the antikick can be understood in terms of the radiation from a deformed black hole where the anisotropic curvature distribution on the horizon correlates with the direction and intensity of the recoil, reproducing the Fitchett distribution. In [34] modifications of the initial data [Eq. (20)] were tested and shown not to produce the expected Fitchett distribution for kicks in the head-on collision of black holes. The results of the present paper also corroborate this interpretation since it reproduces the energy distribution patterns of Davis *et al.* [1] for the case of head-on black holes, consistently extending the case of a particle falling radially into a Schwarzschild black hole.

The cornerstone of our approach is the dependence of the Bondi-Sachs four-momentum wave flux [27] on the news functions—which are the basic quantities characterizing the gravitational wave degrees of freedom of the system and are, by definition, quantities of spin weight $s = -2$ [35,36]. This allows an invariant decomposition into (-2)-spin-weighted modes of the luminosity and of the net momentum flux. This decomposition is exact in the nonlinear regime, leading to an accurate evaluation of the even-parity signals and of their relative contribution to the physical quantities involved in the radiative processes of the system. In this setting we are able to clarify some fundamental new features of the gravitational wave emission in the model.

We organize the paper as follows. In Sec. II, for completeness of the paper, we review some basic characteristics of RT spacetimes including the peeling property of the curvature tensor, which gives an invariant characterization of the radiative nature of the spacetime. In Sec. III we introduce the luminosity and the net momentum flux of the gravitational waves, which are defined in terms of the news function for the axisymmetric case via the BS four-momentum conservation laws; the news function, identified as a quantity of spin weight $s = -2$, is fundamental for our treatment in Secs. V and VI. In Sec. IV we introduce the initial data for the characteristic formalism and discuss its numerical evolution via the RT dynamics by using a Galerkin method. Sections V and VI are the core of the paper: There, we examine the invariant ℓ-mode decomposition of the luminosity and the net momentum flux, and the consequent features of the mode contributions to the total energy and the total impulse carried out of the system by the gravitational waves emitted. Final comments and conclusions are given in Sec. VII.

Except where explicitly stated, throughout the paper we use geometrical units $G = c = 1$.

II. ROBINSON-TRAUTMAN SPACETIMES

RT spacetimes [28,29] are asymptotically flat solutions of Einstein's vacuum equations that describe the exterior gravitational field of a bounded system radiating gravitational waves. The RT metric can be expressed as

$$ds^2 = \alpha^2(u, r, \theta, \phi)du^2 + 2dudr - \frac{r^2}{P^2(u, \theta, \phi)}d\Omega^2, \quad (1)$$

where r is an affine parameter defined along the shear-free null geodesics determined by the vector field $\partial/\partial r$. Here,

$d\Omega^2 = d\theta^2 + \sin^2\theta d\phi^2$. Einstein's equations imply that, in a suitable coordinate system,

$$\alpha^2(u,r,\theta,\phi) = \lambda(u,\theta,\phi) - \frac{2m_0}{r} - 2r\frac{P_{,u}}{P}, \tag{2}$$

where $\lambda(u,\theta,\phi)$ is the Gaussian curvature of the surfaces ($u = \text{const}$, $r = \text{const}$) defined by

$$\lambda = P^2 + \frac{P^2}{\sin\theta}\left(\sin\theta\frac{P_{,\theta}}{P}\right)_{,\theta} + \frac{P^2}{\sin^2\theta}\left(\frac{P_{,\phi}}{P}\right)_{,\phi}, \tag{3}$$

and m_0 is the only dimensional parameter of the spacetime, which fixes the energy and length scales of the system. For the stationary case m_0 corresponds to the rest mass of the black hole with respect to an asymptotic Lorentz frame at future null infinity. The remaining Einstein equations yield

$$12m_0P_{,u} + P^3\left(\frac{(\lambda_{,\theta}\sin\theta)_{,\theta}}{\sin\theta} + \frac{\lambda_{,\phi\phi}}{\sin^2\theta}\right) = 0. \tag{4}$$

In the above, the subscripts u, θ and ϕ preceded by a comma denote derivatives with respect to u, θ and ϕ, respectively. Equation (4), denoted the RT equation, governs the dynamics of the gravitational field [which is totally contained in the metric function $P(u,\theta,\phi)$] and propagates the initial data $P(u_0,\theta,\phi)$ from a given initial characteristic surface $u = u_0$. Chrusciel and Singleton [37] established that RT spacetimes exist globally for all positive $u > u_0$ and converge asymptotically to the Schwarzschild metric as $u \to \infty$, for arbitrary smooth initial data.

The RT equation (4) admits the stationary solution

$$P(\theta,\phi) = (\cosh\gamma + (\mathbf{n}\cdot\hat{x})\sinh\gamma), \tag{5}$$

where γ is a constant. In the above $\hat{x} = (\sin\theta\cos\phi, \sin\theta\sin\phi, \cos\theta)$ is the unit vector along the arbitrary direction $\mathbf{x}$ and $\mathbf{n} = (n_1, n_2, n_3)$ is a constant unit vector (satisfying $n_1^2 + n_2^2 + n_3^2 = 1$). We note that (5) yields $\lambda = 1$, resulting in its stationary character. This solution can be interpreted [25] as a boosted Schwarzschild black hole along the axis determined by the unit vector $\mathbf{n}$ with boost parameter γ, or equivalently, with velocity parameter $v = \tanh\gamma$. The Bondi mass function associated with (5) is $m(\theta,\phi) = m_0/P^3(\theta,\phi)$, and the total mass-energy of this configuration is given by the Bondi mass

$$\begin{aligned} M_B &= (1/4\pi)\int_0^{2\pi} d\phi \int_0^{\pi} m(\theta,\phi)\sin\theta d\theta \\ &= m_0\cosh\gamma = m_0/(\sqrt{1-v^2}). \end{aligned} \tag{6}$$

The two news functions $c_u^{(1)}(u,\theta,\phi)$ and $c_u^{(2)}(u,\theta,\phi)$ of the RT spacetimes can be expressed as [27]

$$c_u^{(1)} + ic_u^{(2)} = \mathcal{L}_{s=-2}P(u,\theta,\phi), \tag{7}$$

where

$$\begin{aligned} \mathcal{L}_{s=-2} = \frac{1}{2}&\left(\partial_{\theta\theta}^2 - \cot\theta\partial_\theta - \frac{1}{\sin^2\theta}\partial_{\phi\phi}^2\right) \\ &+ \frac{i}{\sin\theta}\partial_\phi(\partial_\theta - \cot\theta) \end{aligned} \tag{8}$$

is the operator that transforms scalar spherical harmonics into ($s = -2$)-spin-weighted spherical harmonics [38]. The news functions thus correspond to pure gravitational wave degrees of freedom, characterizing the two polarization modes of the waves, as shown below. We remark that, once we have $P(u,\theta,\phi)$ from the numerical integration of RT equations, the news functions are uniquely determined for all u.

Finally, an important feature of RT spacetimes that establishes its radiative character arises from the expression of its curvature tensor that, in a suitable semi-null tetrad basis [30], assumes the form

$$R_{ABCD} = \frac{N_{ABCD}}{r} + \frac{III_{ABCD}}{r^2} + \frac{II_{ABCD}}{r^3}, \tag{9}$$

where the scalar quantities N_{ABCD}, III_{ABCD} and II_{ABCD} are of the algebraic type N, III and II, respectively, in the Petrov classification of the curvature tensor [39,40], and r is the parameter distance along the principal null direction $\partial/\partial r$. Equation (9) displays the peeling property [40–42] of the curvature tensor, showing that indeed RT is the exterior gravitational field of a bounded source emitting gravitational waves. For large r we have

$$R_{ABCD} \sim \frac{N_{ABCD}}{r}, \tag{10}$$

so that at large r the gravitational field looks like a gravitational wave with propagation vector $\partial/\partial r$. The nonvanishing of N_{ABCD} is an invariant criterion for the presence of gravitational waves, and the asymptotic region where $\mathcal{O}(1/r)$-terms are dominant is defined as the wave zone. The curvature tensor components in the above basis that contribute to N_{ABCD} are $R_{0303} = -R_{0202} = -D(u,\theta)/r + \mathcal{O}(1/r^2)$ and $R_{0203} = -B(u,\theta,\phi)/r + \mathcal{O}(1/r^2)$ where

$$D(u,\theta,\phi) + iB(u,\theta,\phi) = -P^2\partial_u\left(\frac{c_{,u}^{(1)} + ic_{,u}^{(2)}}{P}\right), \tag{11}$$

so $D(u,\theta,\phi)$ and $B(u,\theta,\phi)$ contain all the information on the angular and time dependence of the gravitational wave amplitudes at asymptotic future null infinity [once $P(u,\theta)$ is given for all u]. The news functions will constitute one of the fundamental objects in our analysis.

In the remainder of the paper we deal with head-on mergers along the z axis, so we restrict ourselves to

axisymmetric RT spacetimes having the Killing vector $\partial/\partial\phi$. Accordingly, the formulation will contain one news function only, $c^{(1)}_{,u}(u,\theta)$, from which we now drop the superscript (1). The gravitational waves emitted will have one degree of polarization only.

III. BONDI-SACHS CONSERVATION LAWS AND GRAVITATIONAL WAVE LUMINOSITY

From the supplementary vacuum Einstein equations in the BS integration scheme together with the outgoing radiation condition, the BS four-momentum conservation laws for axisymmetric RT spacetimes are given by (cf. [27] for details)

$$\frac{dP^\mu}{du} = -P^\mu_W(u), \tag{12}$$

where $P^\mu(u)$ is the BS four-momentum defined by

$$P^\mu(u) = \frac{1}{4\pi}\int_0^{2\pi} d\phi \int_0^\pi m(u,\theta) l^\mu \sin\theta d\theta \tag{13}$$

and

$$P^\mu_W(u) = \frac{1}{4\pi}\int_0^{2\pi} d\phi \int_0^\pi \frac{1}{P} l^\mu (c_{,u})^2 \sin\theta d\theta \tag{14}$$

is the net energy-momentum flux carried out by the gravitational waves. In the above the four-vector $l^\mu = (1,0,0,\cos\theta)$ defines the generators of the BMS translations in the temporal and Cartesian z axes of an asymptotic Lorentz frame at future null infinity [43], and

$$c_{,u}(u,\theta) = \frac{1}{2}(\partial^2_{\theta\theta} - \cot\theta\partial_\theta)P(u,\theta) \tag{15}$$

is the news function for the axisymmetric case, cf. (7).

Equation (12) for $\mu = 0$ is the Bondi mass equation [25], the right-hand side of which gives the luminosity of the gravitational waves emitted,

$$L_W(u) = \frac{dE_W(u)}{du} = \frac{1}{2}\int_0^\pi \frac{1}{P}(c_{,u})^2 \sin\theta d\theta. \tag{16}$$

The corresponding energy carried out by gravitational waves at a time $u > u_0$ is

$$E_W(u) = \frac{1}{2}\int_{u_0}^u du \int_0^\pi \frac{1}{P}(c_{,u})^2 \sin\theta d\theta, \tag{17}$$

where u_0 is the initial time. The total gravitational wave energy is given by $E_W(u_f)$, where u_f is the final time (actually the final time of computation) when the gravitational wave emission is considered to have ceased and the system reaches the final configuration of the remnant boosted Schwarzschild black hole.

Equation (12) for $\mu = z$ gives the linear momentum conservation law, the right-hand side of which gives the net momentum flux carried out by the gravitational waves emitted,

$$P^z_W(u) = \frac{1}{2}\int_0^\pi \frac{1}{P}(c_{,u})^2 \cos\theta \sin\theta d\theta, \tag{18}$$

with the associated net gravitational wave impulse

$$I^z_W(u) = \frac{1}{2}\int_{u_0}^u du \int_0^\pi \frac{1}{P}(c_{,u})^2 \cos\theta \sin\theta d\theta. \tag{19}$$

Due to the axisymmetry, the components $P^x_W(u) = 0 = P^y_W(u)$ for all u. We remark that the above quantities are evaluated in a local Lorentz frame at future null infinity of the spacetime. The above equations constitute the basis of our analysis in the paper.

IV. INITIAL DATA AND NUMERICAL EVOLUTION

The initial data to be used were derived in Ref. [30] and can be interpreted as representing two instantaneously Schwarzschild black holes in head-on merger along the z axis, at $u = u_0$,

$$P(u_0,\theta) = \left(\frac{\alpha_1}{\sqrt{\cosh\gamma + \cos\theta\sinh\gamma}} + \frac{\alpha_2}{\sqrt{\cosh\gamma - \cos\theta\sinh\gamma}}\right)^{-2}. \tag{20}$$

For completeness of the paper we summarize and discuss below the basic steps of its derivation as made in [30]. In analogy to bispherical coordinates [44] in the 3-dim Cartesian plane Σ, let us introduce the following parametrization for Cartesian coordinates:

$$x = \frac{a\sin\theta\sinh\eta}{\cosh\eta + \cos\theta\sinh\eta}\cos\phi,$$
$$y = \frac{a\sin\theta\sinh\eta}{\cosh\eta + \cos\theta\sinh\eta}\sin\phi, \tag{21}$$

$$z = \pm\frac{a}{\cosh\eta + \cos\theta\sinh\eta}, \tag{22}$$

for $z > 0$ and $z < 0$, respectively. In the above equations $0 \le \eta \le \infty$, $0 \le \theta \le \pi$, $0 \le \phi \le 2\pi$. In this parametrization, two spheres correspond to each $\eta = \eta_0$, one at $z > 0$ and the other at $z < 0$, centered at $(x = 0,\ y = 0,\ z = \pm a\cosh\eta_0)$, respectively. The Cartesian vector from the origin to a point $P:(x,y,z)$ of Σ has the length

$$r(\eta,\theta)=a\sqrt{\frac{\cosh\eta-\cos\theta\sinh\eta}{\cosh\eta+\cos\theta\sinh\eta}}. \tag{23}$$

The usefulness of this parametrization will become clear in what follows. We note that the Cartesian coordinates are continuous functions, with continuous derivatives, of (η,θ,ϕ). For future reference we introduce the functions

$$S_{\pm}(\eta,\theta)=\sqrt{\cosh\eta\pm\cos\theta\sinh\eta}. \tag{24}$$

The flat space line element $ds^2=(dx)^2+(dy)^2+(dz)^2$ is expressed in the above parametrization as

$$ds^2_{\rm flat}=\frac{a^2}{S^4_{\pm}(\eta,\theta)}[d\eta^2+\sinh^2\eta(d\theta^2+\sin^2\theta d\phi^2)]. \tag{25}$$

We now take Σ as a spacelike surface of initial data, with geometry defined by the line element

$$ds^2=\frac{a^2}{P^2(\eta+\gamma_0,\theta)}[d\eta^2+\sinh^2(\eta+\gamma_0)\times(d\theta^2+\sin^2\theta d\phi^2)], \tag{26}$$

where γ_0 is an arbitrary parameter. By assuming time-symmetric data (namely, Σ, a maximal slice with extrinsic curvature $K_{ab}=0$) we obtain that the Hamiltonian constraints reduce to ${}^{(3)}R=0$. With the substitution $\Phi^2\equiv 1/P$ the constraint equation reduces to the Laplace equation

$$\frac{1}{\sin\theta}(\Phi_\theta\sin\theta)_\theta+(\Phi'\sinh^2(\eta+\gamma_0))'+\frac{3}{4}\sinh^2(\eta+\gamma_0)\Phi=0, \tag{27}$$

where a prime denotes a derivative with respect to η. Obviously the solutions

$$\Phi=\frac{1}{S_{\pm}(\eta+\gamma_0,\theta)} \tag{28}$$

satisfy Eq. (27) and, with respect to the metric (26), correspond to flat space solutions (zero curvature). It then follows that the linear combination

$$\Phi=\left(\frac{\alpha_1}{S_-(\eta+\gamma_0,\theta)}\right)+\left(\frac{\alpha_2}{S_+(\eta+\gamma_0,\theta)}\right) \tag{29}$$

is a nonflat solution of (27), where α_1 and α_2 are arbitrary positive constants. The nonflat 3-dim geometry defined by (29),

$$ds^2=a^2\Phi^4[d\eta^2+\sinh^2(\eta+\gamma_0)\times(d\theta^2+\sin^2\theta d\phi^2)], \tag{30}$$

is asymptotically flat with a form analogous to that of the 3-dim spatial section of the Schwarzschild geometry in isotropic coordinates. In fact, a straightforward calculation shows that the metric (30) can be rewritten as

$$ds^2=\left(\alpha_2+\alpha_1\frac{S_+(\eta+\gamma_0,\theta)}{S_-(\eta+\gamma_0,\theta)}\right)^4 ds^2_{\rm flat}, \tag{31}$$

and for $\eta\gg\gamma_0$ we can express (31) as

$$ds^2=\left(\alpha_2+\frac{a\alpha_1}{r(\eta,\theta)}\right)^4 ds^2_{\rm flat}. \tag{32}$$

To probe the asymptotic structure of (32), let us consider η large and, for this η, points (x,y,z) whose distance from the origin is also large, namely, when $(\eta\to\infty,\ \theta\simeq 0)$. In this instance, returning to Cartesian coordinates, the 3-geometry [Eq. (32)] can be given in the approximate form

$$g_{ij}\simeq\left(1+\frac{2M_S}{r(\eta,\theta)}\right)\delta_{ij}, \tag{33}$$

where M_S is the Schwarzschild mass, $M_S=m_0(\alpha_1+\alpha_2)$. Here we have fixed the scale of the bispherical-type coordinates by taking $a(\alpha_1/\alpha_2)=m_0(\alpha_1+\alpha_2)/2$, where m_0 is a parameter with the dimension of length in geometrical units.

From the above construction we can now extract initial data for the RT dynamics, which has its initial value problem on null characteristic surfaces. Based on initial data formulation on characteristic surfaces proposed by D'Inverno and Stachel [45,46]—in which the degrees of freedom of the vacuum gravitational field are contained in the conformal structure of 2-spheres embedded in a 3-spacelike surface—we are then led to adopt the conformal structure given by the conformal factor (29) defined on the surface $\eta=0$,

$$P(u_0,\theta)=\left(\frac{\alpha_1}{S_-(\gamma_0,\theta)}+\frac{\alpha_2}{S_+(\gamma_0,\theta)}\right)^{-2}, \tag{34}$$

as initial data for RT dynamics. This conformal structure is to be extended along bicharacteristics and propagated along a timelike congruence of the spacetime via RT dynamics. In (20) we dropped the subscript 0 in γ_0. A restricted spacetime can then be constructed locally as the product of the 2-sphere geometry times a timelike plane (u,r), generated by a null vector $\partial/\partial r$ and a timelike vector $\partial/\partial u$, with geometry $d\sigma^2=\alpha^2(u,r,\theta)du^2+2dudr$. The four-geometry is then

$$ds^2=\alpha^2(u,r,\theta)du^2+2dudr-\frac{r^2}{P^2(u,\theta)}\times(d\theta^2+\sin^2\theta d\phi^2). \tag{35}$$

Equation (35) is the RT metric, the dynamics of which (ruled by Einstein's field equations) propagates the initial data (34) forward in time from the characteristic initial surface $u=u_0$. We note that Einstein's vacuum equations

demand that the function $\alpha^2(u,r,\theta)$ has the form given in (2).

The interpretation of the asymptotically flat initial data (34), corresponding to two instantaneously interacting Schwarzschild black holes boosted along the z axis, is now discussed, based on perturbations of the RT metric (35) constructed with such data. As seen in Sec. II, for $\alpha_1 = 0$ the data in (35) correspond to a static Schwarzschild black hole [with the total Bondi mass $m_0(\alpha_2)^6\cosh\gamma_0$] boosted along the negative direction of the z axis with $v = \tanh\gamma_0$. For $\alpha_1 \neq 0$, with $\alpha_1 \ll \alpha_2$, the configuration is no longer static and therefore cannot be a black hole, but it can still be interpreted as an initially perturbed boosted Schwarzschild black hole. Conversely, the same considerations hold for $(\alpha_1 \neq 0,\ \alpha_2 = 0)$ and $\alpha_1 \neq 0$ with $\alpha_2 \ll \alpha_1$, the latter case also corresponding to an initially perturbed boosted black hole. In this sense we associate the perturbation with a black hole of relative small mass boosted along the opposite direction of the larger black hole. The initial infalling velocity of the black holes is defined as $v = \tanh\gamma_0$.

In the derivation of (20) it turns out that $\alpha = \alpha_2/\alpha_1$ is the mass ratio of the Schwarzschild masses of the initial data, as seen by an asymptotic observer. In the remainder of the paper we take $\alpha_1 = 1$ and denote $\alpha_2 = \alpha$ the mass ratio. These data already have a single apparent horizon, so the evolution covers the post-merger regime up to the final configuration, when the gravitational wave emission ceases. For α sufficiently small the data may be considered as a perturbation of a Schwarzschild black hole in the RT dynamics. It is also worth remarking that, in the full Bondi-Sachs problem, further data (the news functions) are needed to determine the evolution of the system. However, for the RT dynamics the news functions are specified once $P(u,\theta)$ is given for all u, cf. (15).

The initial data [Eq. (20)] are evolved numerically via the RT equation (4), which is integrated using a Galerkin method with a Legendre polynomial projection basis space [47] adapted to the axisymmetric RT dynamics. The implementation of the Galerkin method, as well as its accuracy and stability for long time runs, is described in detail in Sec. V of Ref. [48]. The autonomous dynamical system derived via the Galerkin basis projection is integrated using a fourth-order Runge-Kutta recursive method (adapted to our constraints) together with a C++ integrator for a truncation $N = 7$. Exhaustive numerical experiments show that after a sufficiently long time $u \sim u_f$, all the modal coefficients of the Galerkin expansion become constant up to 12 significant digits, corresponding to the final time of computation u_f. At u_f the gravitational wave emission is considered to effectively cease. By numerically reconstructing $P(u,\theta)$ for all $u > u_0$, we can obtain the time behavior of important physical quantities, such as the news functions, the net gravitational wave flux and associated quantities. From the final constant modal coefficients we obtain $P(u_f,\theta)$, which, in all cases, can be approximated as

$$P(u_f,\theta) \simeq P_f(\cosh\gamma_f + \cos\theta\sinh\gamma_f). \tag{36}$$

With the final parameters (P_f,γ_f) obtained from the final modal coefficients, we have, in all cases, that the rms error of Eq. (36) is of the order of, or smaller than, 10^{-12}. The final configuration then corresponds to a Schwarzschild black hole [cf. (5) and (6)] along the z axis with a final boost parameter γ_f and a final Bondi rest mass m_0/P_f^3. In all cases $\gamma_f < \gamma$ and $P_f < 1$.

Except where explicitly stated, in this paper we restrict ourselves to a boost parameter $\gamma = 0.5$ in the initial data [Eq. (20)].

V. MODE DECOMPOSITION OF THE RADIATIVE CONTENT OF GRAVITATIONAL WAVE EMISSION

We are now led to examine the energy carried out of the system by the gravitational waves emitted. As we have seen, from the Bondi energy conservation law we can express the gravitational wave luminosity as [cf. Eq. (16)]

$$L_W(u) = \frac{1}{2}\int_0^\pi \frac{1}{P}(c_{,u})^2\sin\theta d\theta. \tag{37}$$

As already discussed the news function $c_{,u}(\theta,u)$ appearing in the right-hand side of (16) and defined in (15) is an object of spin-weight (-2), while the function $P(u,\theta)$ has zero spin weight; thus, we can make the expansion of $(c_{,u}(\theta,u)/\sqrt{P})$ in the basis of $(s=-2)$-spin-weighted spherical harmonics, cf. (7). Due to the axisymmetry of the problem, this expansion is restricted to the $m = 0$ basis, namely,

$$\left(\frac{c_{,u}(\theta,u)}{\sqrt{P}}\right) = \sum_{\ell\geq 2} N_{\ell 0}(u)\,{}_{-2}\mathcal{Y}_{\ell 0}(\theta), \tag{38}$$

where we define

$${}_{-2}\mathcal{Y}_{\ell 0}(\theta) = \sqrt{\frac{(2\ell+1)(\ell-2)!}{4\pi(\ell+2)!}}(\partial^2_{\theta\theta} - \cot\theta\partial_\theta)P_\ell(\theta), \tag{39}$$

with $\ell \geq 2$ and $P_\ell(\theta)$ the ℓth Legendre polynomial, normalized as

$$2\pi\int_0^\pi {}_{-2}\mathcal{Y}_{\ell 0}(\theta)\,{}_{-2}\mathcal{Y}_{j0}(\theta)\sin\theta d\theta = \delta_{\ell j}. \tag{40}$$

From (16) we then obtain

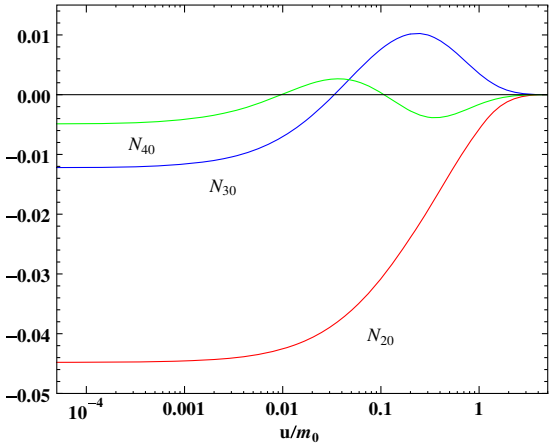

FIG. 1. Plot of the (-2)-spin-weighted modes $N_{\ell 0}(u)$, $\ell = 2, 3$ and 4 corresponding to the decomposition of the total luminosity $L_W(u)$. These modes give the main contribution to the luminosity and to the total radiated energy by gravitational waves. Graph made for the mass ratio $\alpha = 0.025$.

$$L_W(u) = \frac{dE_W(u)}{du} = \frac{1}{4\pi}\sum_{\ell\geq 2} N^2_{\ell 0}(u), \tag{41}$$

where

$$N_{\ell 0}(u) = 2\pi \int_0^\pi \left(\frac{c_{,u}(\theta,u)}{\sqrt{P}}\right)_{-2}\mathcal{Y}_{\ell 0}(\theta)\sin\theta d\theta. \tag{42}$$

Equation (41) gives the mode decomposition of the luminosity (see Fig. 1) and, by an integration up to a time u, we obtain the contribution of each mode to the energy carried out by gravitational waves up to u. The expression (41) is the exact RT equivalent of the Moncrief-Zerilli formula for the radiated luminosity of a particle falling radially into a Schwarzschild black hole [49,50]. Since from our numerical evaluations we can directly have the exact $L_W(u)$ (up to the accuracy of our numerical code) and analogously the $N_{\ell 0}(u)$ [cf. Eqs. (38)–(42)], we can therefore make a clean analysis of the weight of the contribution of each mode to the luminosity L_W and to the energy E_W, as done below. The even-parity character of the waves in our system is connected to the axisymmetry of the system we are examining.

In Fig. 2 (left panel) we display the luminosity $L_W(u)$, obtained numerically from the exact expression (16), on which we superpose the partial sum $\sum_{\ell=2}^{5} N^2_{\ell 0}(u)/4\pi$, which accurately approximates $L_W(u)$, with a normalized rms deviation between the curves $\leq 10^{-2}\%$. The contributions of higher modes $\ell \geq 6$ are negligible. Actually, the dominant contribution to the luminosity comes from the quadrupolar mode $\ell = 2$, as can be seen in Fig. 2 (right panel). The quadrupolar contribution increases from about 84% to 99.7% of the total radiated energy, for mass ratios $\alpha = 0.0125$ and $\alpha = 0.9$, respectively, as discussed below.

Integrating (41) in the whole time domain $[u_0 = 0, u_f]$, where u_f corresponds to the black hole remnant configuration, we obtain the total energy carried out by gravitational waves,

$$E_W^{\text{total}} = \sum_{\ell\geq 2} E_{W\ell}, \tag{43}$$

where

$$E_{W\ell} = \frac{1}{4\pi}\int_{u_0}^{u_f} N^2_{\ell 0}(u)du \tag{44}$$

is the total radiated energy per mode ℓ.

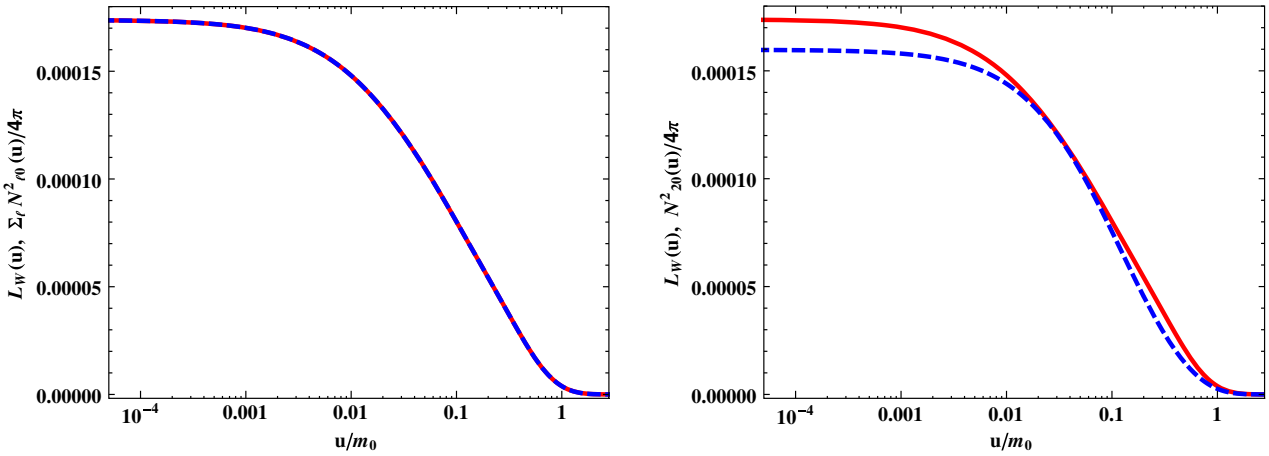

FIG. 2. (Left panel) Plot of the exact luminosity $L_W(u)$ (red continuous curve) on which we superpose the partial sum (41) with $\ell = 2$, 3, 4, 5 (blue dashed curve), for the mass ratio $\alpha = 0.025$. The contributions of higher modes $\ell \geq 6$ are negligible. The normalized rms deviation between the two curves is $\leq 10^{-2}\%$. (Right panel) Plot of the exact luminosity $L_W(u)$ (red continuous curve) and the luminosity of the $\ell = 2$ mode only, namely, $N^2_{20}(u)/4\pi$ (blue dashed curve), showing the dominance of the quadrupolar mode (84%) in the extraction of energy of the system by the gravitational waves emitted.

TABLE I. The radiated energy per mode $E_{W\ell}$ and the relative contribution of each mode to the total radiated energy $E_W^{\rm total}$, for several mass ratios $0.0125 \leq \alpha \leq 0.8$. For small mass ratios we see that about 84% is in the quadrupole ($l = 2$) mode and 14% in the octupole ($l = 3$) mode. As α increases the dominance of the quadrupole mode radiation increases. For large values of α, e.g., $\alpha = 0.8$, we have ~99.5% and ~0.27% in the $l = 2$ and $l = 3$ modes, respectively.

	$\alpha = 0.0125$, $E_W^{\rm total}/m_0 = 7.877839 \times 10^{-6}$		$\alpha = 0.025$, $E_W^{\rm total}/m_0 = 3.257298 \times 10^{-5}$		$\alpha = 0.06$, $E_W^{\rm total}/m_0 = 2.050809 \times 10^{-4}$	
ℓ	$E_{W\ell}/m_0$	$E_{W\ell}/E_W^{\rm total}$	$E_{W\ell}/m_0$	$E_{W\ell}/E_W^{\rm total}$	$E_{W\ell}/m_0$	$E_{W\ell}/E_W^{\rm total}$
2	6.572867×10^{-6}	0.834349	2.736639×10^{-5}	0.840156	1.755436×10^{-4}	0.855972
3	1.102154×10^{-6}	0.139905	4.420647×10^{-6}	0.135715	2.545205×10^{-5}	0.124107
4	1.735627×10^{-7}	0.022032	6.763394×10^{-7}	0.020764	3.567958×10^{-6}	0.012522
5	2.546657×10^{-8}	3.233×10^{-3}	9.584842×10^{-8}	2.943×10^{-3}	4.576429×10^{-7}	2.232×10^{-3}
6	3.426003×10^{-9}	4.349×10^{-4}	1.246684×10^{-8}	3.827×10^{-4}	5.430287×10^{-8}	2.648×10^{-4}
	$\alpha = 0.1$, $E_W^{\rm total}/m_0 = 6.258021 \times 10^{-4}$		$\alpha = 0.2$, $E_W^{\rm total}/m_0 = 3.066076 \times 10^{-3}$		$\alpha = 0.25$, $E_W^{\rm total}/m_0 = 5.253709 \times 10^{-3}$	
ℓ	$E_{W\ell}/m_0$	$E_{W\ell}/E_W^{\rm total}$	$E_{W\ell}/m_0$	$E_{W\ell}/E_W^{\rm total}$	$E_{W\ell}/m_0$	$E_{W\ell}/E_W^{\rm total}$
2	5.466025×10^{-4}	0.873443	2.797298×10^{-3}	0.912338	4.873149×10^{-3}	0.927563
3	6.934556×10^{-5}	0.110811	2.423081×10^{-4}	0.079029	3.458758×10^{-4}	0.065835
4	8.730322×10^{-6}	0.013951	2.403290×10^{-5}	7.838×10^{-3}	3.178859×10^{-5}	0.006051
5	1.004957×10^{-6}	1.606×10^{-3}	2.218168×10^{-6}	7.235×10^{-4}	2.656441×10^{-6}	5.056×10^{-4}
6	1.088764×10^{-7}	1.740×10^{-4}	2.023823×10^{-7}	6.601×10^{-5}	2.231797×10^{-7}	4.248×10^{-5}
	$\alpha = 0.3$, $E_W^{\rm total}/m_0 = 8.2807778 \times 10^{-3}$		$\alpha = 0.4$, $E_W^{\rm total}/m_0 = 1.794259 \times 10^{-2}$		$\alpha = 0.5$, $E_W^{\rm total}/m_0 = 3.261573 \times 10^{-2}$	
ℓ	$E_{W\ell}/m_0$	$E_{W\ell}/E_W^{\rm total}$	$E_{W\ell}/m_0$	$E_{W\ell}/E_W^{\rm total}$	$E_{W\ell}/m_0$	$E_{W\ell}/E_W^{\rm total}$
2	7.782889×10^{-3}	0.939874	1.722167×10^{-2}	0.959820	3.177479×10^{-2}	0.974217
3	4.544982×10^{-4}	5.488593×10^{-2}	6.575541×10^{-4}	0.036648	7.527140×10^{-4}	0.023078
4	4.008497×10^{-5}	4.840726×10^{-3}	5.9468287×10^{-5}	3.314×10^{-3}	8.419377×10^{-5}	2.581×10^{-3}
5	3.048896×10^{-6}	3.681895×10^{-4}	3.6227025×10^{-6}	2.019×10^{-4}	3.716736×10^{-6}	1.139×10^{-4}
6	2.394997×10^{-7}	2.892236×10^{-5}	2.659085×10^{-7}	1.482×10^{-5}	3.005458×10^{-7}	9.215×10^{-6}
	$\alpha = 0.6$, $E_W^{\rm total}/m_0 = 5.442588 \times 10^{-2}$		$\alpha = 0.7$, $E_W^{\rm total}/m_0 = 8.4394487 \times 10^{-2}$		$\alpha = 0.8$, $E_W^{\rm total}/m_0 = 1.239577 \times 10^{-1}$	
ℓ	$E_{W\ell}/m_0$	$E_{W\ell}/E_W^{\rm total}$	$E_{W\ell}/m_0$	$E_{W\ell}/E_W^{\rm total}$	$E_{W\ell}/m_0$	$E_{W\ell}/E_W^{\rm total}$
2	5.357688×10^{-2}	0.984401	8.364351×10^{-2}	0.991102	1.233609×10^{-1}	0.995185
3	7.219961×10^{-4}	0.013265	5.669453×10^{-4}	6.718×10^{-3}	3.335639×10^{-4}	2.690×10^{-3}
4	1.231914×10^{-4}	2.263×10^{-3}	1.808288×10^{-4}	2.143×10^{-3}	2.608761×10^{-4}	2.1046×10^{-3}
5	3.408470×10^{-6}	6.263×10^{-5}	2.631222×10^{-6}	3.118×10^{-5}	1.543681×10^{-6}	1.245×10^{-5}
6	3.916353×10^{-7}	7.196×10^{-6}	5.580596×10^{-7}	6.613×10^{-6}	8.107954×10^{-7}	6.541×10^{-6}

In Table I we give the numerical values of the total radiated energy $E_W^{\rm total}/m_0$ and of the radiated energy $E_{W\ell}/m_0$ (44) per mode $\ell = 2, 3, 4, 5, 6$, evaluated for the mass ratios $0.0125 \leq \alpha \leq 0.8$. We can see that the contribution to the total radiated energy $E_W^{\rm total}$ comes mainly from the quadrupole ($\ell = 2$) and the octupole ($\ell = 3$) modes: for small mass ratios the radiated energy is about 84% in the quadrupole mode and 14% in the octupole mode, while for large values of α, e.g., $\alpha = 0.8$, we have 99.5% and 0.27% in the quadrupole and octupole modes, respectively. In Table II we display the data corresponding to the mass ratios $\alpha = 0.9$ and 1.0. There we still see the dominance of the quadrupole mode in the total emitted energy. Now, however, the contribution of the odd modes $\ell = 3$, 5 is surpassed by the adjacent even modes $\ell + 1 = 4$, 6, respectively (contrary to the pattern seen in Table I). In the limit $\alpha = 1$ the energy in all odd modes is zero, also resulting in a zero total net impulse as discussed in Sec. VI.

For the mass ratios examined in our numerical simulations we obtain that the radiated energy per multipole ℓ decays exponentially with ℓ. This behavior is more accurate as the mass ratio is smaller, as shown below. In Figs. 3 and 4 we display the log-linear plot of the points $E_{W\ell}/m_0$ versus ℓ for $\ell = 2, \ldots, 6$ for several mass ratios $0.0125 \leq \alpha \leq 0.9$. The best-fit curve to these points corresponds to the simple exponential law

$$\log(E_{W\ell}/m_0) = -\mathcal{B}\ell + \mathcal{A}. \tag{45}$$

The parameters $\mathcal{B}$ (the linear coefficient) and $\mathcal{A}$ obtained from the best fit of the points, for $0.0125 \leq \alpha \leq 0.9$, are given in Table III. The normalized rms deviation between the best-fit straight lines and the log-linear plots of the

TABLE II. The radiated energy per mode $E_{W\ell}$ and the relative contribution of each mode to the total radiated energy $E_W^{\rm total}$, for the mass ratios $\alpha = 0.9$ and 1.0. We note that for $\alpha = 0.9$ the relative contribution of the odd modes ($\ell = 3, 5$) is already surpassed by the contribution of the even modes $\ell = 4, 6$ respectively, and for $\alpha = 1.0$ all the odd mode components are zero. This leads to the breaking of the linear correlation in the log-linear plot of the points for these higher mass ratio values.

	$\alpha = 0.9$, $E_W^{\rm total}/m_0 = 1.750733 \times 10^{-1}$		$\alpha = 1.0$, $E_W^{\rm total}/m_0 = 2.399227 \times 10^{-1}$	
ℓ	$E_{W\ell}/m_0$	$E_{W\ell}/E_W^{\rm total}$	$E_{W\ell}/m_0$	$E_{W\ell}/E_W^{\rm total}$
2	1.745982×10^{-1}	0.997286	2.394176×10^{-1}	0.997894
3	2.735963×10^{-5}	1.5627×10^{-4}	0	0
4	3.675352×10^{-4}	2.099×10^{-3}	5.035822×10^{-4}	2.0989×10^{-3}
5	4.924858×10^{-7}	2.8130×10^{-6}	0	0
6	1.155872×10^{-6}	6.6022×10^{-6}	1.590953×10^{-6}	6.6311×10^{-6}

points is $\leq 0.82\%$ for $\alpha \leq 0.3$, increasing to 7% for $\alpha = 0.7$ and with large deviations for higher mass ratios. The last column of Table III contains the normalized rms deviations for all α.

It is remarkable that the exponential pattern of the plots—first observed in the computation by Davis *et al.* [1] (cf. also [51]) of the gravitational radiation from a point test particle falling radially into a Schwarzschild black hole—extends accurately to the nonlinear regime of head-on mergers for mass ratios $\alpha \leq 0.3$. In this sense, for these mass ratios the initial data [Eq. (20)] may be considered to actually correspond to a perturbed Schwarzschild black hole. This exponential behavior is also verified for large values of $0.3 < \alpha \leq 0.7$, with normalized rms deviations $\lesssim 7\%$, cf. Table III. These results are illustrated in Figs. 3 and 4.

The breaking of the exponential behavior appears in the domain of mass ratios $0.8 \leq \alpha \leq 1.0$ as illustrated in Fig. 4

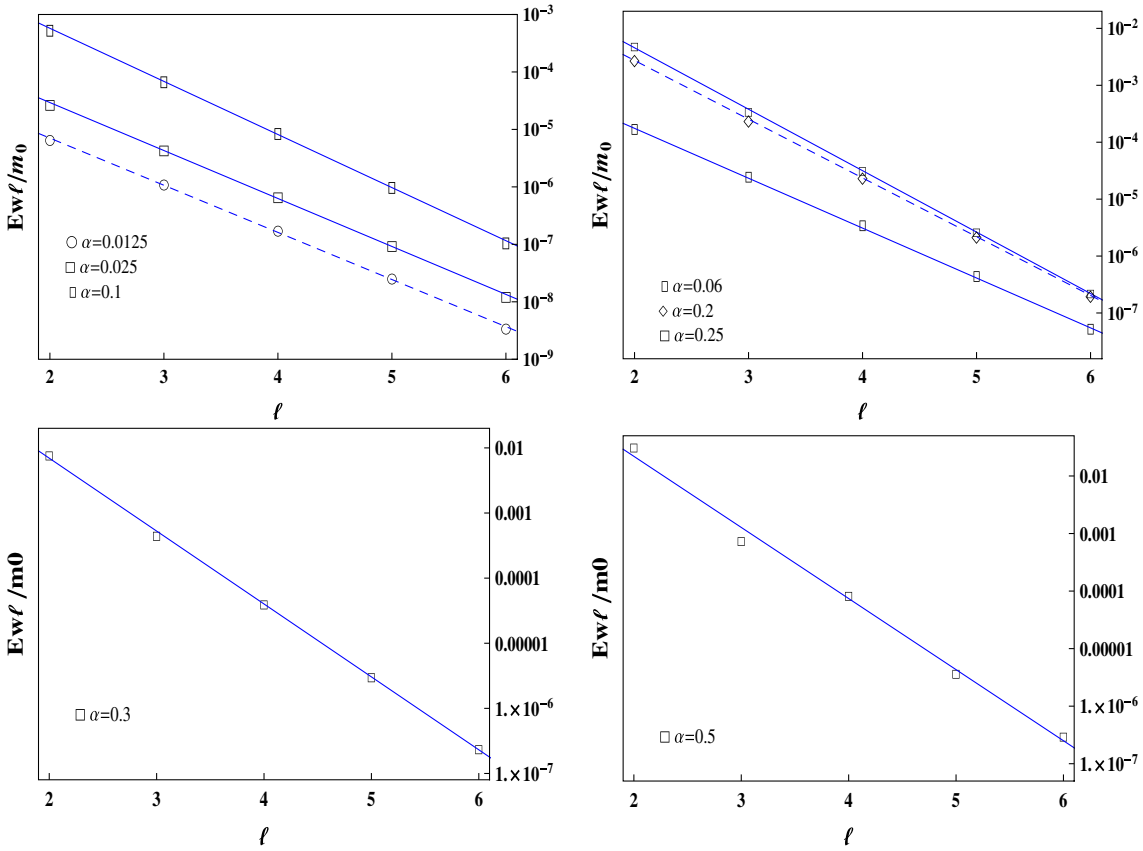

FIG. 3. Log-linear plot of the points $E_{W\ell}/m_0$ (given in Table I) versus ℓ, showing the exponential decay of $E_{W\ell}/m_0$ with ℓ. The parameters corresponding to the best-fit straight lines of the log-linear plots are given in Table III, for the several mass ratios α considered. This pattern—first observed by Davis *et al.* [1] in the gravitational radiation of a point test particle falling radially into a Schwarzschild black hole—is seen to be maintained in the nonlinear regime of head-on merger of two black holes. The graphs for the several mass ratios were separated in four figures to avoid overcluttering.

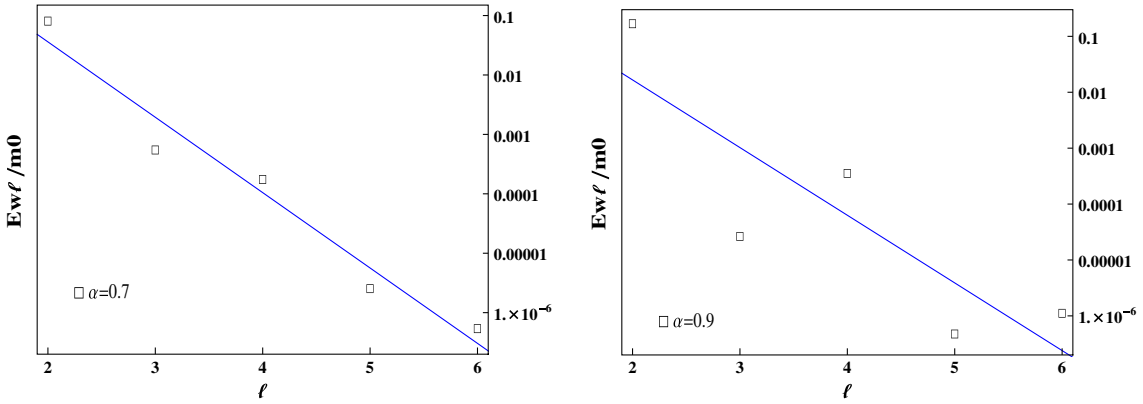

FIG. 4. Log-linear plot of the points $E_{W\ell}/m_0$ versus ℓ for mass ratios $\alpha = 0.7$ and $\alpha = 0.9$. The parameters of the best-fit straight lines of the log-linear plot are given in Table III, together with the normalized rms deviations between the points and the straight lines. We take the case $\alpha = 0.7$ as the acceptable limit for a linear correlation of the points, with a normalized rms $\simeq$7%. The breaking of the linear correlation seen in the case $\alpha = 0.9$ is due to the fact that the contribution of the even modes $\ell = 4$, 6 surpasses that of the odd modes $\ell = 3$, 5, respectively.

(right panel), where we can observe a large deviation in the linear correlation of the log-linear plot of the points for $\alpha = 0.9$. This results from the fact that the contribution of the even modes ($\ell = 4$, 6) to the total emitted energy surpasses that of the odd modes ($\ell = 3$, 6), respectively, cf. Tables II and III and Fig. 5. For $\alpha = 1.0$ all the odd ℓ mode components of the energy are zero; actually, for $\alpha = 1.0$ all odd $N_\ell(u)$ are zero.

Finally, the total radiated energy E_W^{total}/m_0, given in the top lines of Table I for several mass ratios α, exhibits a simple linear relation with α,

$$E_W^{\text{total}}/m_0\alpha^2 = 0.143275\alpha + 0.048462, \qquad (46)$$

as shown in Fig. 6 for $0.01 \le \alpha \le 0.3$. The value for $\alpha = 0.01$ included in the figure and not included in Table I is $E_W^{\text{total}}/(m_0\alpha^2) = 0.0500813$. The straight line is the best fit

TABLE III. The coefficients $\mathcal{A}$ and $\mathcal{B}$ for the best fit of the points to the law [Eq. (45)], shown in Figs. 3 and 4, with the normalized rms deviations between the curves and the points.

α	$\mathcal{A}$	$\mathcal{B}$	nrms deviation
0.0125	−8.0845497	1.888628	0.0080
0.0250	−6.5928280	1.921927	0.0079
0.0600	−2.0180594	2.018059	0.0129
0.1000	−3.2054306	2.127668	0.0058
0.2000	−1.1498687	2.376154	0.0027
0.2500	−0.4200762	2.485164	0.0052
0.300	0.1884550	2.578219	0.0082
0.400	1.1859355	2.735836	0.0158
0.500	1.8704772	2.844801	0.0480
0.600	2.3025239	2.900835	0.0445
0.700	2.5189604	2.920803	0.0700
0.800	2.5450789	2.924088	0.1066
0.900	1.4762816	2.786813	0.2002

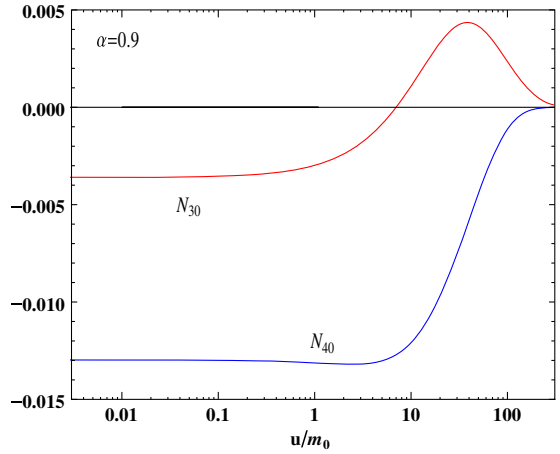

FIG. 5. Plot of the modes $N_{\ell 0}(u)$, $\ell = 3$, 4 for the mass ratio $\alpha = 0.9$, illustrating the decreasing of the energy of odd modes ℓ relative to the respective even modes $\ell + 1$ for mass ratios $\alpha > 0.7$ (cf. Tables I and II). For the limit case $\alpha = 1$ all the $N_{\ell 0}(u)$ for $\ell =$ odd modes are zero.

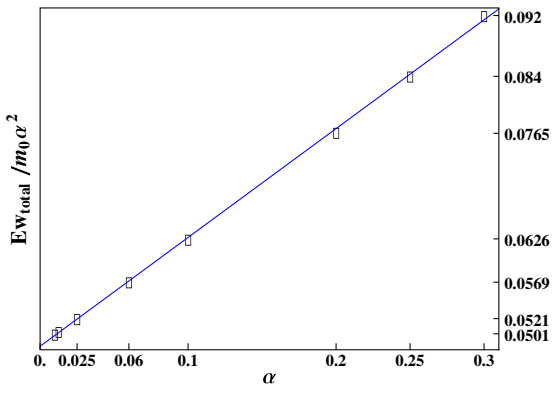

FIG. 6. Plot of the points $(E_W^{\text{total}}/m_0\alpha^2)$ versus α and the best-fit straight line given in (46). The normalized rms deviation between the points and the curve is $\simeq$0.35%.

of the points with a normalized rms deviation ≃0.35%. In the point particle limit ($\alpha \to 0$) we obtain $E_W^{\rm total}/m_0\alpha^2 = 0.04846$, about 5 times larger than the value ∼0.0104 of [1,51]. We should mention that for $\alpha \geq 0.3$ the points deviate from the straight-line behavior.

VI. NET MOMENTUM FLUX AND THE IMPULSE OF GRAVITATIONAL WAVES: ADJACENT-EVEN-ODD MODE MIXING

In the same vein we now examine the net momentum flux and the associate impulse carried out by the gravitational waves. We undertake an analysis of the (−2) spin-weighted mode decomposition of these quantities in the nonlinear regime. We start by the expression of the net momentum flux along the z axis given by (18),

$$P_W^z(u) = \frac{1}{2}\int_0^\pi \frac{1}{P}(c_{,u})^2 \cos\theta \sin\theta d\theta,$$

and (i) taking into account that the news is an object of spin weight $s = -2$, and (ii) using the mode expansion (38), we may express (18) as

$$P_W^z(u) = \frac{1}{2}\sum_{\ell\geq 2}\sum_{j\geq 2} N_{\ell 0}(u)N_{j0}(u) \times \int_{-1}^{1} {}_{-2}\mathcal{Y}_{\ell 0}(x)\,{}_{-2}\mathcal{Y}_{j0}(x)x dx, \quad (47)$$

where $x = \cos\theta$. The integral appearing in the right-hand side of (47) results in

$$\int_{-1}^{1} {}_{-2}\mathcal{Y}_{\ell 0}(x)\,{}_{-2}\mathcal{Y}_{j0}(x)x dx = \frac{c_\ell}{2\pi}\delta_{\ell,j\pm 1},$$

where the nonzero coefficients c_ℓ (for $\ell = j \pm 1$) are given by

$$c_\ell = \sqrt{\frac{(\ell+3)(\ell-1)}{(2\ell+1)(2\ell+3)}}. \quad (48)$$

For reference, numerical values of these coefficients are given in Table IV with the precision of six decimals.

It therefore follows that only the coupling of adjacent-even-odd modes contributes to the total net momentum flux according to

TABLE IV. The mixed-mode impulses $I^z_{W(\ell,\ell+1)}$ and the relative contribution of each mode to the total impulse $I^z_W(u_f)$, for several mass ratios in the domain $0.0125 \leq \alpha \leq 0.9$. The mode-mixed impulses decrease exponentially with ℓ, as seen in Figs. 8. The data show that about 80%–83% of the total impulse comes from the contribution of the quadrupole-octupole mixed mode (2,3), for small α's, increasing to ∼95% for higher α's. The mixed-mode impulses reach a maximum at $\alpha \simeq 0.7$.

		$\alpha = 0.0125$, $I^z_W(u_f)/m_0 = -1.999697\times10^{-6}$		$\alpha = 0.1$, $I^z_W(u_f)/m_0 = -1.3695603\times10^{-4}$	
$(\ell,\ell+1)$	c_ℓ	$I^z_{W(\ell,\ell+1)}/m_0$	$I^z_{W(\ell,\ell+1)}/I^z_W(u_f)$	$I^z_{W(\ell,\ell+1)}/m_0$	$I^z_{W(\ell,\ell+1)}/I^z_W(u_f)$
(2,3)	0.377964	-1.596427×10^{-6}	0.798334	-1.143631×10^{-4}	0.835035
(3,4)	0.4364358	-3.390364×10^{-7}	0.169544	-1.964248×10^{-5}	0.143422
(4,5)	0.460566	-5.511852×10^{-8}	0.027563	-2.607581×10^{-6}	0.019039
(5,6)	0.473050	-8.062786×10^{-9}	4.032×10^{-3}	-3.095024×10^{-7}	2.260×10^{-3}
(6,7)	0.480384	-1.001698×10^{-9}	5.009×10^{-4}	-3.193502×10^{-8}	2.332×10^{-4}
		$\alpha = 0.3$, $I^z_W(u_f)/m_0 = -1.209250\times10^{-3}$		$\alpha = 0.5$, $I^z_W(u_f)/m_0 = -3.029662\times10^{-3}$	
$(\ell,\ell+1)$	c_ℓ	$I^z_{W(\ell,\ell+1)}/m_0$	$I^z_{W(\ell,\ell+1)}/I^z_W(u_f)$	$I^z_{W(\ell,\ell+1)}/m_0$	$I^z_{W(\ell,\ell+1)}/I^z_W(u_f)$
(2,3)	0.377964	-1.08852×10^{-3}	0.900161	-2.833056×10^{-3}	0.93511
(3,4)	0.4364358	-1.103185×10^{-4}	0.091229	-1.8220256×10^{-4}	0.0601396
(4,5)	0.460566	-9.573314×10^{-6}	7.9167×10^{-3}	-1.347608×10^{-5}	0.004448
(5,6)	0.473050	-7.778460×10^{-7}	6.4325×10^{-4}	-8.701113×10^{-7}	2.872×10^{-4}
(6,7)	0.480384	-5.854250×10^{-8}	4.841×10^{-5}	-5.5684998×10^{-8}	1.838×10^{-5}
		$\alpha = 0.7$, $I^z_W(u_f)/m_0 = -4.192803\times10^{-3}$		$\alpha = 0.9$, $I^z_W(u_f)/m_0 = -2.614904\times10^{-3}$	
$(\ell,\ell+1)$	c_ℓ	$I^z_{W(\ell,\ell+1)}/m_0$	$I^z_{W(\ell,\ell+1)}/I^z_W(u_f)$	$I^z_{W(\ell,\ell+1)}/m_0$	$I^z_{W(\ell,\ell+1)}/I^z_W(u_f)$
(2,3)	0.377964	-3.993392×10^{-3}	0.9524397	-2.507183×10^{-3}	0.958805
(3,4)	0.4364358	-1.8426886×10^{-4}	0.043949	-9.906382×10^{-5}	0.037884
(4,5)	0.460566	-1.432440×10^{-5}	3.4164×10^{-3}	-8.234415×10^{-6}	3.1490×10^{-3}
(5,6)	0.473050	-7.664367×10^{-7}	1.8280×10^{-4}	-3.948353×10^{-7}	1.5099×10^{-4}
(6,7)	0.480384	-5.002935×10^{-8}	1.1932×10^{-5}	-2.737432×10^{-8}	1.04686×10^{-5}

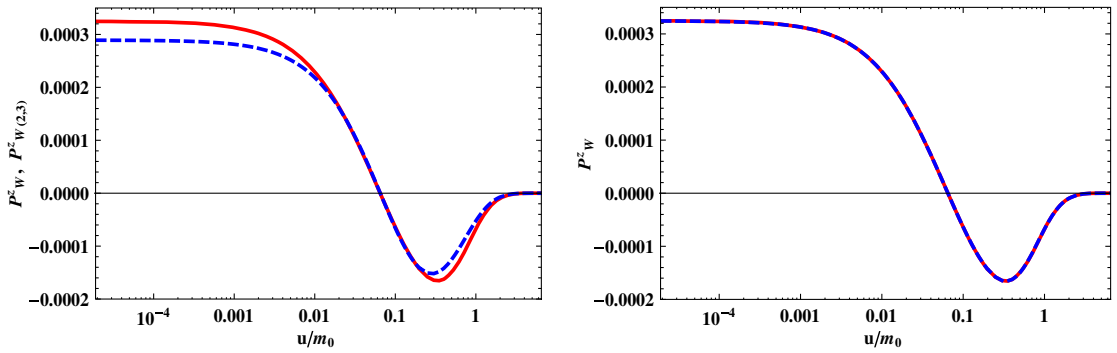

FIG. 7. (Left panel) Plot of the total net gravitational wave momentum flux $P^z_W(u)$ (red continuous line) together with its mode-mixed component $P^z_{W_{(2,3)}}(u)$ (dashed blue line), which corresponds to about 84% of the total impulse of the gravitational wave signal. (Right panel) Superposition of $P^z_W(u)$ (red continuous line) with the partial sum, right-hand side of (49) for $\ell = 2, 3, 4$, illustrating a proper convergence of the series; the normalized rms deviation of the two curves is ∼0.35%. Plots for the mass ratio $\alpha = 0.1$.

$$P^z_W(u) = \sum_{\ell\geq 2} P^z_{W_{(\ell,\ell+1)}} \tag{49}$$

where

$$P^z_{W_{(\ell,\ell+1)}} = \frac{c_\ell}{2\pi} N_{\ell 0}(u) N_{\ell+1,0}(u). \tag{50}$$

In Fig. 7 we display the net momentum flux $P^z_W(u)$ and the mode-mixed component

$$P^z_{W_{(2,3)}}(u) = \frac{c_2}{2\pi} N_{20}(u) N_{30}(u),$$

evaluated numerically for the mass ratio $\alpha = 0.1$. This first component of the expansion (49), $P^z_{W_{(2,3)}}$, turns out to be the dominant term of the expansion, corresponding to about 83% of the total gravitational wave impulse for this mass ratio. We see that the system undergoes an initial acceleration along the positive z axis, due to the initial positive phase of $P^z_W(u)$, cf. Fig. 7 (right panel), followed by a dominant decelerated phase that lasts until the boosted black hole remnant configuration is attained, as evaluated in an asymptotic Lorentz frame at future null infinity. This corresponds to a final negative net impulse imparted to the system by the gravitational waves emitted, resulting in a net kick velocity measured in an asymptotic zero-initial-Bondi-momentum frame, as discussed below.

Integrating Eq. (12) in time, we obtain the momentum conservation law of the system,

$$P^z(u) - P^z(u_0) = -I^z_W(u) \tag{51}$$

where

$$I^z_W(u) = \int_{u_0}^{u} P^z_W(u) du \tag{52}$$

is the impulse imparted on the system by the gravitational waves carried out of the system up to a time u. From (49) we then obtain

$$I^z_W(u_f) = \sum_{\ell\geq 2} I^z_{W(\ell,\ell+1)} = \sum_{\ell\geq 2} \frac{c_\ell}{2\pi} \int_{u_0}^{u_f} N_{\ell 0}(u) N_{\ell+1,0}(u) du, \tag{53}$$

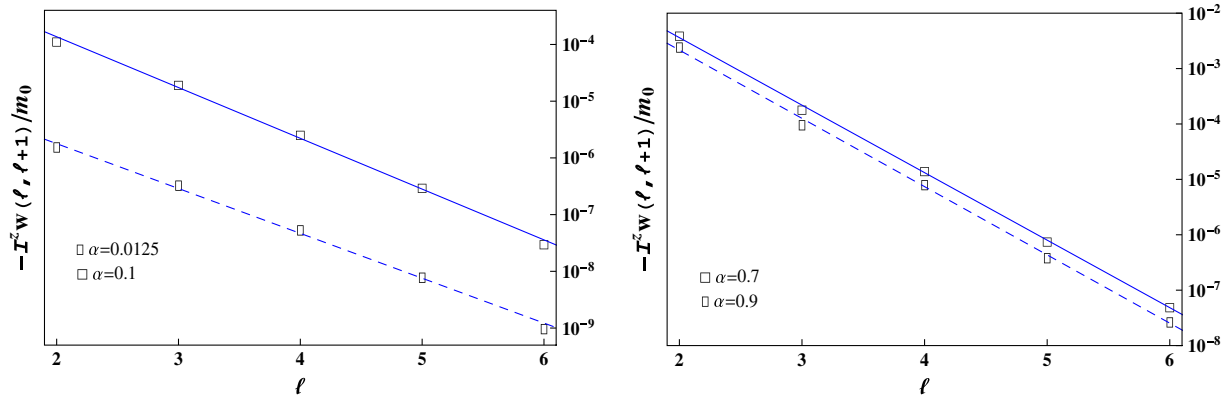

FIG. 8. Log-linear plots of the mixed-mode impulses $-I^z_{W(\ell,\ell+1)}/m_0$ versus ℓ, given in Table IV, for the mass ratios $\alpha = 0.0125$, 0.1, 0.7 and 0.9. The points are accurately fitted by straight lines in the whole range of α, showing the exponential decay of the impulses with ℓ. The maximum occurs at about $\alpha = 0.7$, after which the impulses decrease, as illustrated by the distribution for $\alpha = 0.9$. We note that the total impulse is zero for the equal-mass case $\alpha = 1.0$.

TABLE V. The coefficients $\mathcal{A}$ and $\mathcal{B}$ for the best fit of the points to the law [Eq. (54)], from the data of Table IV and illustrated in Fig. 8, and the normalized rms deviations between the curves and the points.

α	$\mathcal{Q}$	$\mathcal{P}$	nrms deviation
0.0125	−9.4686510	1.848650	0.0193
0.1000	−4.7968411	2.0517345	0.0167
0.300	−1.7960712	2.461575	0.0081
0.500	−0.4624912	2.701856	0.0032
0.700	−0.0105959	2.805748	0.0087
0.900	−0.4647250	2.837518	0.0128

which corresponds to the mode decomposition of the total net impulse into adjacent-even-odd mixed modes $I^z_{W(\ell,\ell+1)}$, which can be evaluated from the $N_\ell(u)$ obtained in the decomposition (38) of the news function. We remark that the left-hand side of (53) can be evaluated independently, so we may obtain the impulse per mode $I^z_{W(\ell,\ell+1)}$ and the accurate relative contribution of each $(\ell,\ell+1)$ mixed mode to the total net impulse imparted to the system.

The mixed-mode impulses $I^z_{W(\ell,\ell+1)}$ are given in Table IV for several mass ratios in the domain $0.0125 \le \alpha \le 0.9$, together with the relative contribution of each $(\ell,\ell+1)$ mixed mode to the total impulse imparted on the system by the gravitational waves emitted. For the mass ratio domain $0.0125 \le \alpha \le 1.0$ examined in our numerical simulations, we obtain that the gravitational wave impulse per mixed mode $(\ell,\ell+1)$ decays exponentially with ℓ. This behavior is accurately verified for the whole domain of mass ratios examined, even for higher mass ratios, e.g., $\alpha = 0.9$, differing in this latter case of the energy behavior. The (2,3)-mixed-mode contributions to the total impulses are dominant, contributing with approximately 83% for small mass ratios, e.g., $\alpha = 0.1$, and with ∼95% for higher mass ratios, e.g., $\alpha = 0.9$. At about $\alpha = 0.7$ we can see that the total impulses reach a maximum. For $\alpha > 0.7$ the gravitational wave impulse mixed modes decrease. We should note, however, that for $\alpha = 1.0$ the total impulse and its mixed-mode components are zero. This is due to the fact that all the odd modes N_ℓ of the news functions are zero for $\alpha = 1$, as expected from the symmetry of the system for the equal-mass case.

In Fig. 8 we display the log-linear plots of the impulses $-I^z_{W(\ell,\ell+1)}/m_0$ versus ℓ given in Sec. IV, corresponding to the mass ratios $\alpha = 0.0125$, 0.1, 0.7 and 0.9. The best-fit curves to the points are the straight lines,

$$\log(-I^z_W(u_f)/m_0) = -\mathcal{P}\ell + \mathcal{Q}. \tag{54}$$

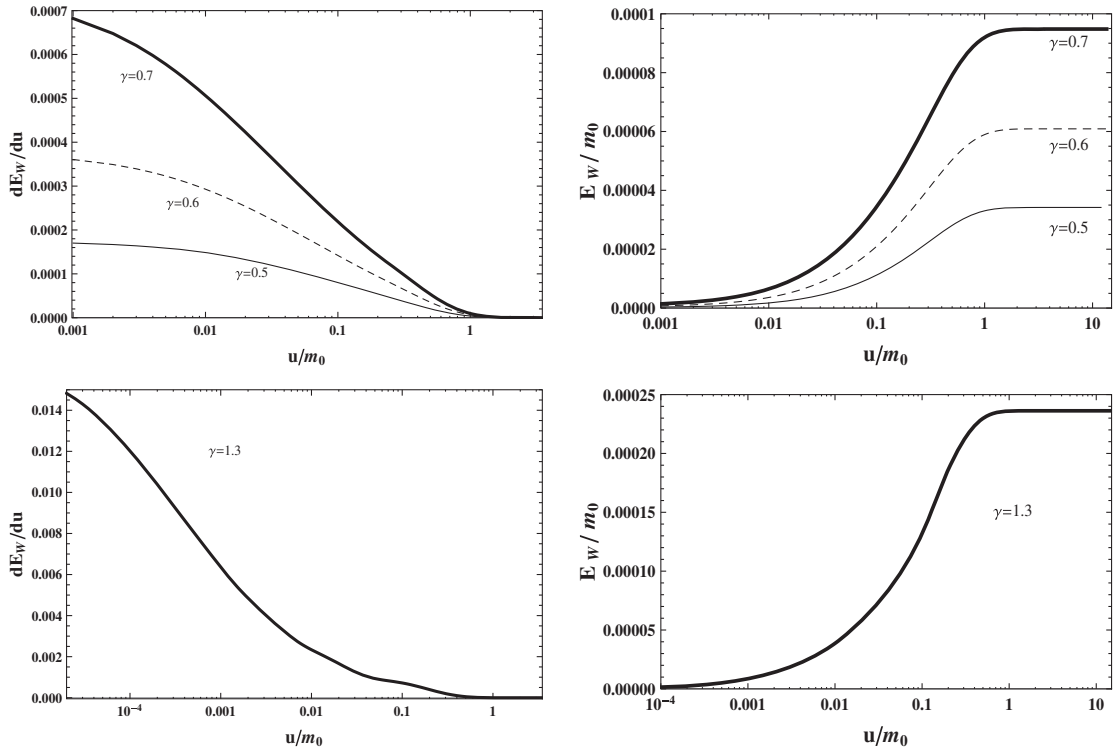

FIG. 9. Plot of the luminosity (left panels) and of the energy carried out by the gravitational waves (right panels) for increasing boost parameters $\gamma = 0.5$, 0.6, 0.7, 0.9 and 1.3. We see that the head-on mergers become more energetic as γ increases, while the time duration of the gravitational wave bursts $\Delta u/m_0 \simeq 2$ remains approximately constant with increasing γ. Plots are made for the mass ratio $\alpha = 0.025$.

The values of the best-fit coefficients $\mathcal{P}$ and $\mathcal{Q}$ corresponding to the numerical data of Table IV are given in Table V, together with the normalized rms deviations of the linear law (54). This illustrates the above-mentioned exponential decay of the mixed-mode impulses with ℓ for the whole mass ratio domain.

From the total impulse $I^z_W(u_f)$ we define the net kick velocity of the system, in an asymptotic zero-initial-Bondi-momentum frame, as

$$V_k = \frac{-cI^z_W(u_f)P_f^3}{m_0} \tag{55}$$

where m_0/P_f^3 is the Bondi rest mass of the remnant black hole (cf. Sec. IV), with the velocity of light c restored. For illustration we obtain $V_k \simeq 0.56$ km/s and $V_k \simeq 24.55$ km/s for the mass ratios $\alpha = 0.0125$ and 0.1, respectively. Also the mixed-mode $(\ell, \ell+1)$ components of these kick velocities can be analogously calculated with the data from Table IV, using the values $P_f \simeq 0.978163819$ and $P_f \simeq 0.842322219$ evaluated numerically for $\alpha = 0.0125$ and 0.1, respectively.

This mode-mixing effect for the total momentum fluxes and the associated recoil velocities was first reported by Moncrief [23] for small odd-parity axisymmetric perturbations in the Oppenheimer-Snyder collapse models, and by Lousto and Price [24] for even-parity axisymmetric perturbations on a Schwarzschild black hole by a particle falling radially.

Finally, we have also checked the dependence of the luminosity and of the energy carried out by the gravitational waves on the boost parameter γ. The head-on merger of two black holes becomes more energetic as γ increases, while the time duration of the bursts of gravitational waves $\Delta u/m_0 \simeq 2$ appears not to change with the increase of γ. These results are illustrated in Fig. 9, for $\gamma = 0.5$, 0.6, 0.7, and 1.3. For reasons of accuracy we restricted the numerical evaluations up to $\gamma = 1.3$ (corresponding to $v \sim 0.86$). For larger γ's the exact initial data [Eq. (20)] becomes greatly deformed; therefore, for these γ's the expansion of the initial data in the basis of the Galerkin projection space is not sufficiently accurate in our present numerical code. For $\gamma = 1.3$ we obtain an integrated error between the exact data and its basis expansion $\lesssim 10^{-4}$, while the error associated with lower γ's is $\lesssim 10^{-7}$ [48].

VII. FINAL COMMENTS AND CONCLUSIONS

In this paper we examine gravitational wave radiative patterns in the head-on merger of two black holes with initial mass ratios $0.01 \leq \alpha \leq 1.0$, using the Bondi-Sachs characteristic formalism in the realm of Robinson-Trautman (RT) dynamics. From the Bondi-Sachs energy-momentum conservation laws, we construct the luminosity (the energy flux) $L_W(u) = dE_W(u)/du$ as well as the net momentum flux $P^z_W(u)$ of the gravitational waves emitted by the system, given in terms of the news function which is a (-2)-spin-weighted object connected to the basic degrees of freedom of the system. The news function can be obtained from the numerical integration of the RT equation for all times u up to the final time of computation u_f when the gravitational wave emission ceases and the black hole remnant configuration is attained. It is worth mentioning that in the Bondi-Sachs formalism adopted here, all the physical quantities involved in the radiative processes of gravitational waves in the system are correctly evaluated at future null infinity of the spacetime, as expected.

In the above formalism we obtain a (-2)-spin-weighted ℓ mode decomposition of the luminosity, which corresponds to the exact RT equivalent of the Moncrief-Zerilli formula for the radiated luminosity of even-parity linear waves [49,50]. The dominant contribution to the total luminosity actually comes from the $\ell = 2$ quadrupolar mode. Integrating this formula in the whole time domain $u = [0, u_f]$, we obtain the total radiated energy E_W/m_0 and the energy radiated out per mode ℓ for mass ratios $0.0125 \leq \alpha \leq 1.0$. For small mass ratios the radiated energy is about 84% in the quadrupole mode and 14% in the octupole mode, while for large values of α, e.g., $\alpha = 0.8$, we have 99.5% and 0.27% in the quadrupole and octupole modes, respectively. Accordingly, the radiated energy contributed by higher modes is smaller, decreasing with the increase of the mass ratio. However, we should remark that for higher mass ratios, e.g., $\alpha = 0.9$, the radiated energy contributed by even modes surpasses that of odd modes, so in the limit $\alpha = 1.0$ the energy radiated in odd modes is zero. The latter property is also connected with the fact that the total gravitational wave impulse is zero for the equal-mass case due to the adjacent-mode-mixing effect in the structure of the momentum modes.

For the mass ratios considered in this paper we obtain that the radiated energy per multipole ℓ decays exponentially with ℓ. This remarkable pattern—first observed in the calculation of Davis *et al.* [1] of the gravitational radiation from a point test particle falling radially into a Schwarzschild black hole—extends accurately to the nonlinear regime of head-on mergers of black holes for mass ratios up to $\alpha = 0.3$. In this sense the initial data [Eq. (20)] may be considered to actually correspond to a nonlinearly perturbed Schwarzschild black hole. This exponential behavior was also verified for large values of $0.3 < \alpha \leq 0.7$. The normalized rms deviations increase but remain bounded, $\lesssim 7\%$. The breaking of the exponential behavior appears in the domain of mass ratios $0.8 \leq \alpha \leq 1.0$ and results from the fact that the contributions of the even modes to the total emitted energy surpasses that of the odd-mode contributions. For $\alpha = 1.0$ all odd modes are zero.

We have also made an analogous mode analysis for the net momentum flux and the net impulse carried out by the

gravitational waves. The remarkable feature of the mode decomposition of both the net momentum flux $P^z_W(u)$ and the total net impulse $I^z_W(u_f)$ is the adjacent-even-odd mode mixing pattern in these quantities. We obtained that the gravitational wave impulse contributed by each $(\ell, \ell+1)$ mixed mode also accurately satisfies the exponential decay with ℓ, for the whole mass ratio domain considered, $0.0125 < \alpha < 1$. The (2,3)-mixed-mode contributions to the total impulses are dominant, contributing with approximately 83% for small mass ratios, e.g., $\alpha = 0.1$, and with ~95.8% for higher mass ratios, e.g., $\alpha = 0.9$. At about $\alpha = 0.7$ the total impulses reach a maximum. For $\alpha > 0.7$ the gravitational wave impulse mixed modes decrease. We should note, however, that for $\alpha = 1.0$ the total impulse and its mixed-mode components are zero. This is due to the fact that all the odd modes N_ℓ of the news functions are zero for $\alpha = 1$, as expected from the symmetry of the system for the equal-mass case. Of course, this mode-mixing effect is also present in the decomposition of the net kick velocity imparted to the system by the gravitational wave emission.

Finally, for head-on mergers of two boosted black holes with a relatively small mass ratio, the radiative regime of gravitational wave emission is associated with short bursts of gravitational waves. For example, for a boost parameter $\gamma = 0.5$ and mass ratio $\alpha = 0.06$, the total energy is $E_W \sim 2.0 \times 10^{-4} m_0$ emitted in a period of time $\Delta u \sim 2.17 m_0$. For a black hole system with $m_0 \sim 100 M_\odot$, the process corresponds to a total energy $E_W \sim 3.6 \times 10^{52}$ergs emitted in a time interval $\Delta u \sim 10^{-3}$ sec, which are typical of a gamma-ray burst. However, as α increases the period of time during which the total energy is emitted increases. For instance, if we compare the mode coefficients $N_\ell(u)$ shown in Figs. 1 and 5, for $\alpha = 0.025$ and $\alpha = 0.9$, respectively, we have that the duration of signals differs by 2 orders of magnitude.

We finally remark that the ℓ dominance in the time signals at the wave zone, $m_0 D(u,\theta)$, is distinct from the ℓ dominance of the gravitational wave luminosity and of the radiated energy shown in this paper. In fact, the total emitted energy by gravitational waves when written in terms of the amplitude at the wave zone,

$$E_W(u) = \frac{1}{4\pi}\int_0^u du' \int_0^{2\pi} d\phi \int_0^{\pi} \sin\theta d\theta \left(\int^{u'} \frac{1}{P^2} D du'' \right)^2,$$

is proportional to the flux of the time integral of the equivalent wave-zone Poynting vector, contrary to the case of electrodynamics [27,52].

ACKNOWLEDGMENTS

The authors acknowledge the partial financial support of CNPq/MCTI-Brazil, through Grant No. 151396/2013-2 (R. F. A.), Research Grant No. 304064/2013-0 (I. D. S.), as well as support from FAPES-ES-Brazil (E. V. T.). We are grateful to the anonymous referees whose comments and criticisms allowed us to substantially improve the paper.

[1] M. Davis, R. Ruffini, W. H. Press, and R. H. Price, Phys. Rev. Lett. **27**, 1466 (1971).
[2] B. Abbott *et al.* (LIGO Scientific Collaboration), Rep. Prog. Phys. **72**, 076901 (2009).
[3] G. M. Harry and LIGO Scientific Collaboration, Classical Quantum Gravity **27**, 084006 (2010).
[4] T. Accadia, F. Acernese, F. Antonucci, P. Astone, G. Ballardin *et al.*, Classical Quantum Gravity **28**, 114002 (2011).
[5] K. Somiya (KAGRA Collaboration), Classical Quantum Gravity **29**, 124007 (2012).
[6] J. G. Baker, J. Centrella, D. Choi, M. Koppitz, R. van Meter, and M. C. Miller, Astrophys. J. **653**, L93 (2006).
[7] D. Merrit, M. Milosavljević, M. Favata, S. S. Hughes, and D. E. Holz, Astrophys. J. **607**, L9 (2004).
[8] M. Favata, S. A. Hughes, and D. E. Holz, Astrophys. J. **607**, L5 (2004).
[9] L. Blanchet, Living Rev. Relativ. **9**, 4 (2006).
[10] F. Pretorius, Phys. Rev. Lett. **95**, 121101 (2005).
[11] J. G. Baker, J. Centrella, D. I. Choi, M. Koppitz, and J. van Meter, Phys. Rev. Lett. **96**, 111102 (2006).
[12] M. Campanelli, C. O. Lousto, P. Marronetti, and Y. Zlochower, Phys. Rev. Lett. **96**, 111101 (2006).
[13] J. A. González, U. Sperhake, B. Brügmann, M. Hannam, and S. Husa, Phys. Rev. Lett. **98**, 091101 (2007).
[14] J. A. González, U. Sperhake, and B. Brügmann, Phys. Rev. D **79**, 124006 (2009).
[15] C. F. Sopuerta, N. Yunes, and P. Laguna, Phys. Rev. D **74**, 124010 (2006); **75**, 069903(E) (2007).
[16] A. Le Tiec, L. Blanchet, and C. M. Will, Classical Quantum Gravity **27**, 012001 (2010).
[17] C. O. Lousto, H. Nakano, Y. Zlochower, and M. Campanelli, Phys. Rev. Lett. **104**, 211101 (2010); H. Nakano, Y. Zlochower, C. O. Lousto, and M. Campanelli, Phys. Rev. D **84**, 124006 (2011); C. O. Lousto and Y. Zlochower, Phys. Rev. Lett. **106**, 041101 (2011).
[18] S. Bernuzzi and A. Nagar, Phys. Rev. D **81**, 084056 (2010).
[19] A. Nagar, T. Damour, and A. Tartaglia, Classical Quantum Gravity **24**, S109 (2007).
[20] S. Bernuzzi, A. Nagar, and A. Zenginoglu, Phys. Rev. D **83**, 064010 (2011).

[21] T. Damour and A. Nagar, Phys. Rev. D **76**, 064028 (2007).
[22] S. Bernuzzi, A. Nagar, and A. Zenginoglu, Phys. Rev. D **84**, 084026 (2011).
[23] V. Moncrief, Astrophys. J. **238**, 333 (1980).
[24] C. O. Lousto and R. H. Price, Phys. Rev. D **69**, 087503 (2004).
[25] H. Bondi, M. G. J. van der Berg, and A. W. K. Metzner, Proc. R. Soc. A **269**, 21 (1962).
[26] R. K. Sachs, Proc. R. Soc. A **270**, 103 (1962).
[27] R. F. Aranha, I. Damião Soares, and E. V. Tonini, Classical Quantum Gravity **30**, 025014 (2013).
[28] I. Robinson and A. Trautman, Phys. Rev. Lett. **4**, 431 (1960).
[29] I. Robinson and A. Trautman, Proc. R. Soc. A **265**, 463 (1962).
[30] R. F. Aranha, I. Damião Soares, and E. V. Tonini, Phys. Rev. D **81**, 104005 (2010).
[31] S. Bernuzzi, A. Nagar, and A. Zenginoğlu, Phys. Rev. D **84**, 084026 (2011).
[32] R. F. Aranha, I. Damião Soares, and E. V. Tonini, Phys. Rev. D **82**, 104033 (2010).
[33] L. Rezzolla, R. P. Macedo, and J. L. Jaramillo, Phys. Rev. Lett. **104**, 221101 (2010).
[34] J. L. Jaramillo, R. P. Macedo, P. Moesta, and L. Rezzolla, Phys. Rev. D **85**, 084030 (2012).
[35] E. T. Newman and R. Penrose, J. Math. Phys. (N.Y.) **7**, 863 (1966).
[36] J. N. Goldberg, A. J. MacFarlane, E. T. Newman, F. Rohrlich, and E. C. G. Sudarshan, J. Math. Phys. (N.Y.) **8**, 2155 (1967).
[37] P. Chruściel, Commun. Math. Phys. **137**, 289 (1991); P. Chruściel and D. B. Singleton, Commun. Math. Phys. **147**, 137 (1992).
[38] T. W. Baumgarte and S. L. Shapiro, *Numerical Relativity: Solving Einstein's Equations in the Computer* (Cambridge University Press, Cambridge, England, 2010).
[39] A. Z. Petrov, Sci. Nat. Kazan State University **114**, 55 (1954); reprinted in Gen. Relativ. Gravit. **32**, 1665 (2000).
[40] F. A. E. Pirani, Introduction to Gravitational Radiation Theory, in *Lectures on General Relativity*, Brandeis Summer Institute in Theoretical Physics (Prentice-Hall, New Jersey, 1964), Vol. 1.
[41] R. Sachs, Proc. R. Soc. Edinburgh, Sect. A **264**, 309 (1961); E. T. Newman and R. Penrose, J. Math. Phys. (N.Y.) **3**, 566 (1962).
[42] E. T. Newman and R. Penrose, J. Math. Phys. (N.Y.) **3**, 566 (1962).
[43] R. K. Sachs, Phys. Rev. **128**, 2851 (1962).
[44] G. Arfken, *Mathematical Methods for Physicists* (Academic Press, New York, 1968), Sec. II.14.
[45] R. A. D'Inverno and J. Stachel, J. Math. Phys. (N.Y.) **19**, 2447 (1978); R. A. D'Inverno and J. Smallwood, Phys. Rev. D **22**, 1233 (1980).
[46] J. A. Vickers, in *Approaches to Numerical Relativity*, edited by R. A. D'Inverno (Cambridge University Press, Cambridge, England, 1992), p. 59.
[47] C. A. J. Fletcher, *Computational Galerkin Methods* (Springer, Berlin, 1984).
[48] R. F. Aranha, I. Damião Soares, and E. V. Tonini, Phys. Rev. D **85**, 024003 (2012).
[49] V. Moncrief, Ann. Phys. (Berlin) **88**, 323 (1974).
[50] C. O. Lousto and R. H. Price, Phys. Rev. D **56**, 6439 (1997).
[51] E. Mitsou, Phys. Rev. D **83**, 044039 (2011).
[52] L. Smarr, *Sources of Gravitational Radiation*, edited by L. Smarr (Cambridge University Press, Cambridge, England, 1978), p. 245.